Electric Field-Driven Coherent Spin Reorientation of Optically Generated Electron Spin Packets in InGaAs

S. Kuhlen,[1,2] K. Schmalbuch,[1,2] M. Hagedorn,[1,2] P. Schlammes,[1,2] M. Patt,[1,2] M. Lepsa,[2,3] G. Güntherodt,[1,2] and B. Beschoten[1,2,*]

[1]*II. Physikalisches Institut, RWTH Aachen University, 52056 Aachen, Germany*
[2]*JARA-Fundamentals of Future Information Technology, Jülich-Aachen Research Alliance, Germany*
[3]*Peter Grünberg Institut (PGI-9), Forschungszentrum Jülich GmbH, 52425 Jülich, Germany*

(Received 7 July 2011; revised manuscript received 17 July 2012; published 4 October 2012)

Full electric-field control of spin orientations is one of the key tasks in semiconductor spintronics. We demonstrate that electric-field pulses can be utilized for phase-coherent $\pm\pi$ spin rotation of optically generated electron spin packets in InGaAs epilayers detected by time-resolved Faraday rotation. Through spin-orbit interaction, the electric-field pulses act as local magnetic field pulses. By the temporal control of the local magnetic field pulses, we can turn on and off electron spin precession and thereby rotate the spin direction into arbitrary orientations in a two-dimensional plane. Furthermore, we demonstrate a spin-echo-type spin drift experiment and find an unexpected partial spin rephasing, which is evident by a doubling of the spin dephasing time.

DOI: 10.1103/PhysRevLett.109.146603 PACS numbers: 72.25.Fe, 42.50.Md, 76.30.Pk, 78.47.−p

Most device concepts in semiconductor spintronics rely on the efficient generation of spin-polarized carriers and their phase sensitive manipulation and readout. Initial experiments comprised ferromagnet-semiconductor hybrid structures, where the ferromagnet is either used as a source of spin-polarized carriers [1–3] or as a spin-sensitive detector using magneto-resistive readout [4]. In recent years, however, a new pathway towards spintronics without ferromagnets has evolved, which allows us to generate and to manipulate spins by electric fields E only [5,6]. In ordinary nonmagnetic semiconductors, dc E fields can generate spins by two complementary effects, the spin Hall effect [7–12] and the so-called current induced spin polarization (CISP) [13–16]. Both result from the spin-orbit (SO) coupling. The spin Hall effect leads to a spin accumulation transverse to the current flow direction by spin dependent scattering [9], while CISP is manifested by a uniform spin polarization in the semiconductor, which has been demonstrated both by static and by time-resolved magneto-optical probes [14]. Although the microscopic origin of CISP is not fully understood [13,17–19], in most systems electron spins get oriented along the effective internal magnetic field B_{int}, which can be tuned by the E field strength through SO coupling. Internal magnetic fields have also been determined in 2D electron gases by Shubnikov-de Haas oscillations [20,21], antilocalization [22], photo current [23], static Hanle [24,25], and time-resolved Faraday rotation (TRFR) measurements [26,27]. The control of B_{int} is of fundamental importance for spin manipulation. It can be realized by gate voltages in 2D electron gases [28] or by dc E fields [29,30]. These SO fields have been used by Kato *et al.* to induce spin precession at zero external magnetic field B_{ext} [30].

In this Letter, we report on TR electrical spin manipulation experiments of electron spins in InGaAs. Coherent spin packets are optically generated by circularly polarized laser pump pulses. Their initial spin direction is manipulated by E field pulses, which act as effective local magnetic field pulses (LMFP) due to SO coupling. Using TRFR, we probe the Larmor precession of spin packets induced by the SO field pulse. By changing the pulse width and polarity, we are able to rotate the spins into arbitrary directions within a two-dimensional plane. In addition to spin precession, the E field pulses also yield a lateral drift of the spin packet over several μm. As sign reversal of the pulses will reverse both spin precession and drift direction, we are able to explore spin echo of the spin packet in the diffusive spin transport regime.

Our studies were performed on a 500 nm thick $In_{0.07}Ga_{0.93}As$ epilayer grown on semi-insulating (100) GaAs by molecular beam epitaxy. The room temperature carrier density was set to $n \sim 3 \times 10^{16}$ cm^{-3} by Si doping to allow for long spin dephasing times at low temperatures [31,32]. By chemical wet etching a 140 μm wide and 680 μm long transport channel was patterned and contacted with standard Au/Ge/Ni electrodes. For spin manipulation experiments, the electric field was applied along the $[01\bar{1}]$ crystal axis (or x axis) as shown in Fig. 1(a). For our samples, this configuration yields the strongest CISP with internal magnetic fields pointing along the [011] or y axis (see also Ref. [14]). The device is embedded in a coplanar wave guide and connected to microwave probes [33]. In the following, we discuss two classes of experiments: (I) In static CISP, we will use dc E fields to probe the E field-induced spin polarization measuring the Faraday rotation θ_F in polar geometry (along the [100] or z axis). From the shape of the resulting Hanle depolarization curves we are able to directly extract the internal magnetic field strength $\mathbf{B}_{\mathrm{int}}$ at noncollinear alignment of

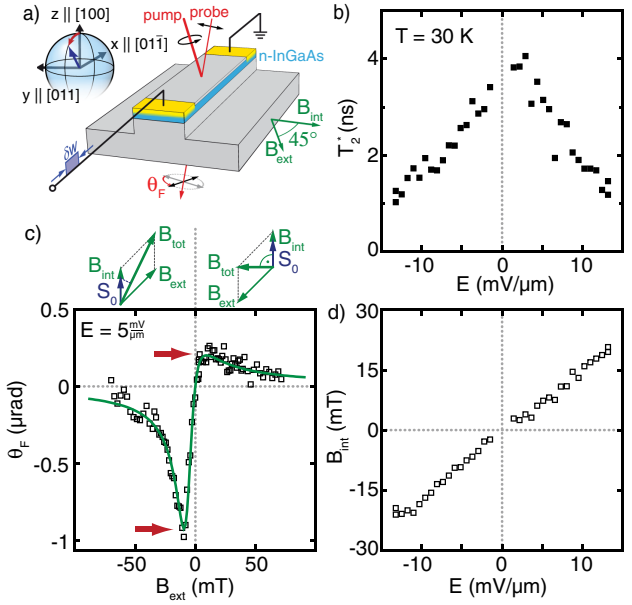

FIG. 1 (color online). (a) Schematic setup. dc or pulsed E fields are applied along the $[01\bar{1}]$ direction of an n-InGaAs transport channel. Electrically or optically generated spins are probed by static and TRFR in polar geometry. (b) T_2^* vs dc E field. (c) (upper panel) Schematics of total effective magnetic field $\mathbf{B}_{\text{tot}}$ for positive and negative B_{ext}. (lower panel) Asymmetric Hanle curve taken at $E = +5\ \frac{\text{mV}}{\mu\text{m}}$ and $T = 30$ K. The green line is a fit to Eq. (1). (d) B_{int} determined from asymmetric Hanle signal vs dc E field.

$\mathbf{B}_{\text{int}}$ with the external magnetic field $\mathbf{B}_{\text{ext}}$ [see Fig. 1(a)]. (II) In TRFR experiments, we use circularly polarized ps laser pump pulses to trigger electron spin coherence in InGaAs. Spin precession about the vector sum of $\mathbf{B}_{\text{int}}$ and $\mathbf{B}_{\text{ext}}$ is probed by a second time-delayed linearly polarized probe pulse using TRFR measurements. $\mathbf{B}_{\text{int}}$ can either result from dc or pulsed electric fields. The latter stems from a pulse-pattern generator, which is synchronized to the picosecond pump laser and is used for time-resolved spin reorientation and spin-echo-type experiments [33].

We first use dc CISP to determine the direction of $\mathbf{B}_{\text{int}}$ and its magnitude in our InGaAs structures. With $\mathbf{B}_{\text{int}}$ being not perpendicular to $\mathbf{B}_{\text{ext}}$ ($\alpha = \angle(\mathbf{B}_{\text{ext}}, \mathbf{B}_{\text{int}}) \neq 90°$) the symmetry of the otherwise expected antisymmetric Hanle curve is broken. For example in Fig. 1(c), the amplitude of $|\theta_F|$ at its extremal values varies by a factor of 3 [see arrows in Fig. 1(c)], which can be attributed to the influence of $\mathbf{B}_{\text{int}}$ on the precession axis and frequency as the spins precess about $\mathbf{B}_{\text{tot}}$ [25]. As illustrated at the top of Fig. 1(c), the respective magnitudes of $\mathbf{B}_{\text{tot}}$ differs for $\pm\mathbf{B}_{\text{ext}}$ and the angle between $\mathbf{B}_{\text{tot}}$ and the initial spin orientation $\mathbf{S}_0$ changes significantly.

Assuming $\mathbf{B}_{\text{int}} \perp z$ and $\mathbf{S}_0 \parallel \mathbf{B}_{\text{int}}$, we can model [33] the Hanle curves by

$$\theta_F(\mathbf{B}_{\text{ext}}) = \theta_0 \frac{\mathbf{B}_{\text{ext}} \sin\alpha}{\mathbf{B}_{1/2}} \left[1 + \left(\frac{\mathbf{B}_{\text{tot}}}{\mathbf{B}_{1/2}}\right)^2\right]^{-1}, \qquad (1)$$

with amplitude $\theta_0 \propto S_0$, the total effective magnetic field $\mathbf{B}_{\text{tot}} = \mathbf{B}_{\text{int}} + \mathbf{B}_{\text{ext}}$ and the angle α between $\mathbf{B}_{\text{ext}}$ and $\mathbf{B}_{\text{int}}$ (i.e., 45°). The width of the Hanle curve $B_{1/2}$ is a direct measure of the transverse dephasing time $T_2^* = (g\frac{\mu_B}{\hbar}B_{1/2})^{-1}$.

The Hanle curves can be fitted according to Eq. (1) (see green curve in Fig. 1(c)). As seen in Fig. 1(b), we observe a strong decrease of T_2^* for both E field polarities, which has also been observed in Ref. [14] indicating additional E field dependent spin dephasing. The extracted B_{int} values in Fig. 1(d) vary almost linearly with the E field and vanish at $E = 0$ (see also Ref. [26]). These internal magnetic fields will be used next for coherent spin manipulation.

For this purpose, coherent electron spin ensembles are generated along the z direction by circularly polarized picosecond laser pump pulses [32,34] and detected by TRFR in polar geometry. The E field will now be used for TR spin manipulation. We note that the E field pulse itself can also create a phase triggered coherent spin polarization, which can be probed by TR-CISP [14]. This effect is, however, negligible as the fraction of spin polarization by CISP is 3 orders of magnitude less than the spin polarization obtained after optical orientation.

We first explore the influence of dc E fields on the coherent spin ensemble in Figs. 2(a) and 2(b) at $B_{\text{ext}} = 0$ and 15 mT, respectively. From these experiments it is obvious that SO induced electron spin precession can be triggered by electrical means. In the former case, for both negative and positive E fields of the same magnitude the spins precess with equal Larmor frequencies $\omega_L = g\frac{\mu_B}{\hbar}B_{\text{tot}}$, where g is the electron g-factor, μ_B Bohr's magneton, and $\hbar$ Planck's constant. In contrast, in the latter case [see Fig. 2(b)] spin precession is accelerated for $E < 0\ \frac{\text{mV}}{\mu\text{m}}$ while it is slowed down for $0 < E < 7.5\ \frac{\text{mV}}{\mu\text{m}}$. This dependence proves the reversal of the $\mathbf{B}_{\text{int}}$ direction upon sign reversal of E. For $E = 0\ \frac{\text{mV}}{\mu\text{m}}$ multiple spin precessions can be observed due to the enhanced T_2^*.

All TRFR data can be described by an exponentially damped cosine function

$$\theta_F(\Delta t) = \theta_0 \exp\left(-\frac{\Delta t}{T_2^*}\right)\cos(\omega_L \Delta t + \delta), \qquad (2)$$

with amplitude θ_0, pump-probe delay Δt and phase δ. This way we can determine T_2^* and B_{int}, which are plotted vs E in Figs. 2(c) and 2(d), respectively. We note a strong decrease of T_2^*, which limits the observable spin coherence. The decrease of T_2^* has previously been assigned to spins drifting out of the probe laser focus [30]. However, as the dephasing times extracted from the above CISP measurements [cf. to Fig. 1(b)] exhibit a similar decrease with the E field, we attribute this effect to additional spin dephasing, which will be evaluated in more detail below by using E pulses for spin manipulation. B_{int} values from TRFR depend also nearly linearly on the E field [Fig. 2(d)]. The nonlinear behavior around $E = 0$ results from non-Ohmic

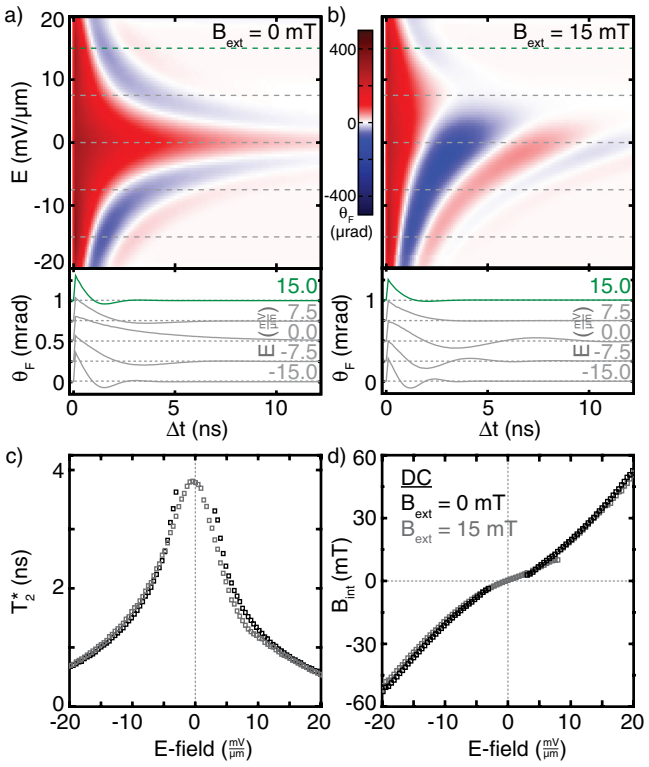

FIG. 2 (color online). TRFR after optical spin orientation in InGaAs ($T = 30$ K). Electron drift in an E field induces B_{int}, which results in spin precession about $\mathbf{B}_{\text{tot}} = \mathbf{B}_{\text{int}} + \mathbf{B}_{\text{ext}}$, shown for (a) $B_{\text{ext}} = 0$ mT and (b) $B_{\text{ext}} = 15$ mT. TRFR scans are plotted in the lower parts at selected E fields. An offset is added for clarity. The resulting parameters (c) T_2^* and (d) B_{int} are in good agreement with the values extracted from Hanle measurements [Figs. 1(b) and 1(d)].

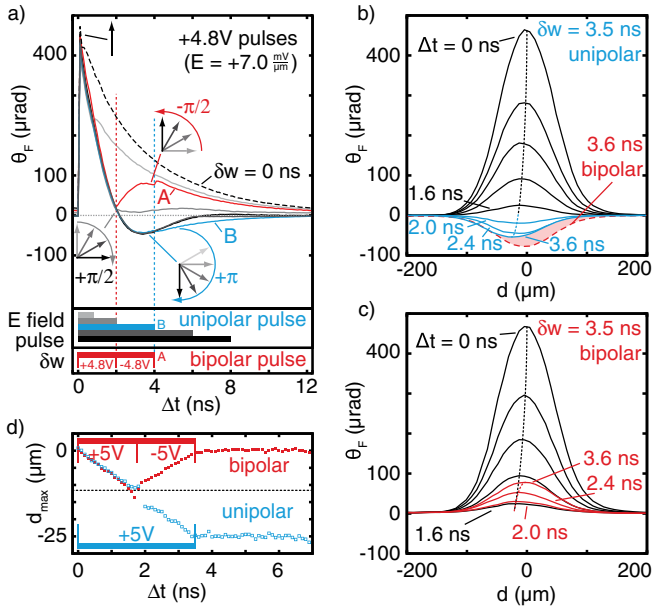

FIG. 3 (color online). Spin manipulation by unipolar and bipolar E field pulses. All E field pulses start at $\Delta t = 0$ ns. (a) TRFR measurements of optically created spin packets ($T = 30$ K), which precess at $B_{\text{ext}} = 0$ during E field pulses of different width δw, which is visualized in the lower panel. Spatiotemporal evolution of spin packet after spin manipulation by (b) unipolar and (c) bipolar pulse. The temporal spacing is 0.4 ns. The final spin distribution at $\Delta t = 3.6$ ns in (c) has been reversed and added as a dashed line in (b). (d) Spatiotemporal drift of spin packet after spin manipulation with unipolar (blue) and bipolar (red) pulses of equal pulse width and magnitude.

contact resistance as seen by the linear dependence of B_{int} on I (not shown).

While in the above dc experiments we can control the spin precession frequency by E fields only, we now want to manipulate the phase of the optically generated coherent spin packet. In other words, we will use E field pulses both to initialize and to stop spin precession at $B_{\text{ext}} = 0$ mT. When the E field pulse reaches the optically generated spin packet, it will create a LMFP for the duration of the pulse. This LMFP will trigger spin precession in the zx plane [see Fig. 1(a)]. The precession frequency depends on the E field strength, while the total precession time is given by the pulse width δw. In Fig. 3(a), we show a sequence of TRFR measurements of optically generated coherent spin packets, which are manipulated by E field pulses of $E = 7$ $\frac{\text{mV}}{\mu\text{m}}$ and various pulse widths ranging from 0 to 8 ns. As expected, we observe spin precession for long pulses of 8 ns (black curve). As the laser repetition time is 12 ns, this case is close to the dc Hanle limit [Fig. 2(a)]. For shorter pulse widths, θ_F always follows this spin precession curve during the field pulse. However, spin precession abruptly stops after the pulse has turned off with elapsed δw. This is seen by a simple exponential decay thereafter, which is observed for all pulse widths. The minimum in θ_F at 3.7 ns shows that the LMFP of 4 ns operates as π pulse [blue curve B in Fig. 3(a)], which rotates the spins by 180° from the $+z$ into the $-z$ direction [35]. The difference between a decaying signal after a 4 ns pulse and further precession (i.e., for 6 and 8 ns pulses) is clearly visible.

As discussed in Fig. 2(d), reversing the E field polarity will reverse B_{int}, which results in a reversal of the spin precession direction. When using a bipolar pulse sequence, which consists of two subsequent pulses with opposite polarity and equal width and magnitude, we expect spin reorientation of the spin packet to its original direction at the end. The red curve A in Fig. 3(a) shows spin manipulation by a bipolar pulse sequence with the same magnitude (4.8 V) and total width (4 ns) as the blue curve B for spin manipulation by a unipolar pulse. During the first 2 ns, both unipolar and bipolar pulses rotate the spin packet by $\pi/2$ into the sample plane. While spin precession for the unipolar pulse will continue to π rotation, spin precession is reversed during the subsequent 2 ns for bipolar pulses, which function as $-\pi/2$ pulses. Remarkably, at 4 ns the value $|\theta_F|$ is larger for the bipolar pulse than for the unipolar pulse but less than the value obtained for free

decay of the ensemble (see dashed black curve for $\delta w = 0$). As $|\theta_F|$ is a direct measure of the net spin moment, its increase indicates partial spin rephasing.

To exclude that the different amplitudes result from the E field-induced drift of the spin packet away from the probe laser spot, we show a series of spatiotemporal profiles of the spin packet in Figs. 3(b) and 3(c) after unipolar and bipolar spin manipulation, respectively. The data have been taken by scanning the probe relative to the pump beam along the E field direction. While the spin packet drifts continuously to the left for unipolar pulses, it reverses the drift direction after 2 ns for bipolar pulses and returns to its original position thereafter [see also Fig. 3(d)]. To better compare the final spin distributions at 3.6 ns for both manipulation schemes, we added the respective curve from Fig. 3(c) with reversed sign as a red dashed line in Fig. 3(b). Despite their small difference in peak positions, the dashed red curve has an overall larger magnitude showing that drift effects are too small to account for the difference in amplitudes and that the observed effect is indeed caused by rephasing.

In the following, we extract spin dephasing times for both spin manipulation experiments to further quantify the effect of spin rephasing. For each E field value, we have measured TRFR for pulse widths ranging from 200 ps to 10 ns. In Figs. 4(a) and 4(b), we show the respective θ_F vs Δt curves on false color plots for unipolar and bipolar pulses with $|E| = 7\ \frac{\mathrm{mV}}{\mu\mathrm{m}}$. The solid black lines mark the end of the pulses. The resulting θ_F after spin manipulation is plotted vs $\delta w_{\mathrm{total}}$ in Fig. 4(c) (blue curve for unipolar pulses and red curve for bipolar pulses). These data are taken at 200 ps after the end of each pulse [see dotted lines in Figs. 4(a) and 4(b)]. Spin precession can be observed for unipolar pulses for pulse widths above 2 ns [see also Fig. 3]. In contrast, no spin precession or sign reversal of θ_F is seen for bipolar pulses. Instead, θ_F is exponentially decaying unambiguously demonstrating that the spin packet points along the original direction after the bipolar pulse sequence. We also included in Fig. 4(c) additional TRFR traces at selected E field values which have been extracted by the same method. It is obvious that θ_F from spins precessing continuously in one direction (unipolar pulse) decays much faster than the signal stemming from bipolar pulses. This is most clearly seen for large E field values. The extracted spin dephasing times are depicted in Fig. 4(d). As expected, spin dephasing during the unipolar pulses (blue open circles) matches values from the above dc case (filled squares). In contrast, spin dephasing times after bipolar spin manipulation are longer at all E fields demonstrating that the bipolar pulse sequence allows for spin-echo studies of the spin ensemble in diffusive transport. The observed spin rephasing is strongest at the largest E fields where the spin dephasing times doubles.

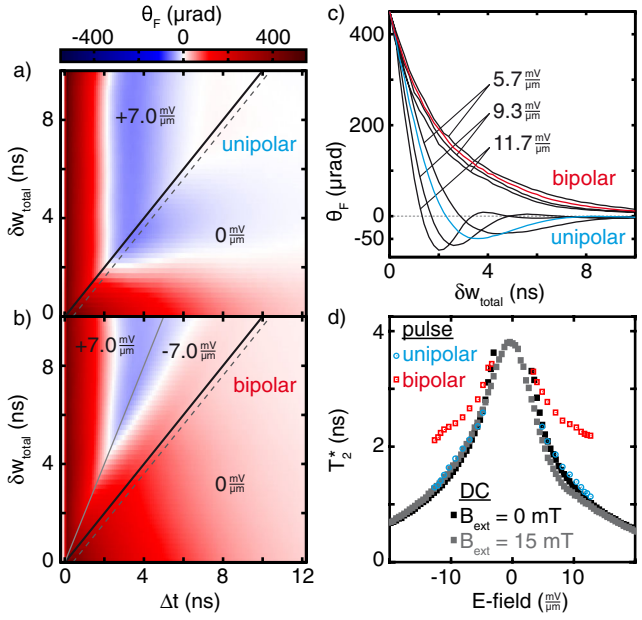

FIG. 4 (color online). False color plots of TRFR measurements for spin manipulation by (a) unipolar and (b) bipolar E field pulse with variable pulse width δw. The end of the pulses is marked by solid lines. (c) $\theta_F(\Delta t = \delta w + 200\ \mathrm{ps})$ vs δw from traces along dashed lines in (a) and (b). (d) T_2^* taken from fits to curves in (c). T_2^* values during unipolar pulses agree with results from dc E fields [cf. to Fig. 2(c)], while T_2^* after bipolar pulses shows partial rephasing.

Our findings show that the E field induced decrease of T_2^* is partly caused by spin dephasing and not by spin relaxation. During Larmor precession, a phase spreading is built up when the LMFP is applied, which might result from local fluctuation of B_{int} across the spin packet. In contrast to standard spin-echo techniques, we reverse the precession direction by changing the LMFP polarity. As the spin ensemble now precesses in the opposite direction, it can partially compensate for the accumulated phase spreading. However, this is only true if the variation in precession frequencies is identical for both drift directions for the individual spins. We note that the observed spin rephasing is not expected for Elliott-Yafet spin scattering [36] as spin-flip events, which occur during momentum scattering will destroy time-reversal symmetry. In contrast, spin scattering due to the D'yakonov-Perel' mechanism [37] occurs between momentum scattering events by spin precession about the k-dependent spin-orbit field. As momentum scattering occurs on ps time scales [38], which is shorter than T_2^* by 3 orders of magnitude, the ensemble phase will be randomized during transport for each momentum scattering event. As individual electrons will not follow their identical paths during the spin-echo pulse they will precess about different spin-orbit fields, which also should not result in spin rephasing in diffusive transport.

In conclusion, we have shown to achieve full time-resolved electrical phase control of electron spin packet orientation within a 2D plane in InGaAs in zero magnetic field. A novel spin-echo technique has been used to explore electric field-induced spin dephasing, which surprisingly

revealed that partial rephasing is possible even in diffusive spin transport. Some of us have shown recently that linearly polarized light can be utilized to achieve full 2D control of the initial spin direction [34]. Adding the electric field-driven spin rotation to this new technique, we expect being able to achieve full 3D control of the spin orientation [39], which could provide an important step toward all-electrical spintronics without ferromagnets.

We acknowledge useful discussion with F. Hassler. This work was supported by DFG through FOR 912.

*bernd.beschoten@physik.rwth-aachen.de

[1] Y. Ohno, D. K. Young, B. Beschoten, F. Matsukura, H. Ohno, and D. D. Awschalom, Nature (London) **402**, 790 (1999).
[2] S. A. Crooker, M. Furis, X. Lou, C. Adelmann, D. L. Smith, C. J. Palmstrom, and P. A. Crowell, Science **309**, 2191 (2005).
[3] G. Kioseoglou, A. T. Hanbicki, J. M. Sullivan, O. M. J. van 't Erve, C. H. Li, S. C. Erwin, R. Mallory, M. Yasar, A. Petrou, and B. T. Jonker, Nature Mater. **3**, 799 (2004).
[4] X. Lou, C. Adelmann, S. A. Crooker, E. S. Garlid, J. Zhang, K. S. M. Reddy, S. D. Flexner, C. J. Palmstrom, and P. A. Crowell, Nature Phys. **3**, 197 (2007).
[5] D. Awschalom and N. Samarth, Physics **2**, 50 (2009).
[6] Y. Kato, R. C. Myers, D. C. Driscoll, A. C. Gossard, J. Levy, and D. D. Awschalom, Science **299**, 1201 (2003).
[7] J. E. Hirsch, Phys. Rev. Lett. **83**, 1834 (1999).
[8] S. Zhang, Phys. Rev. Lett. **85**, 393 (2000).
[9] Y. K. Kato, R. C. Myers, A. C. Gossard, and D. D. Awschalom, Science **306**, 1910 (2004).
[10] J. Wunderlich, B. Kaestner, J. Sinova, and T. Jungwirth, Phys. Rev. Lett. **94**, 047204 (2005).
[11] V. Sih, R. C. Myers, Y. K. Kato, W. H. Lau, A. C. Gossard, and D. D. Awschalom, Nature Phys. **1**, 31 (2005).
[12] E. S. Garlid, Q. O. Hu, M. K. Chan, C. J. Palmstrom, and P. A. Crowell, Phys. Rev. Lett. **105**, 156602 (2010).
[13] V. M. Edelstein, Solid State Commun. **73**, 233 (1990).
[14] Y. K. Kato, R. C. Myers, A. C. Gossard, and D. D. Awschalom, Phys. Rev. Lett. **93**, 176601 (2004).
[15] N. P. Stern, S. Ghosh, G. Xiang, M. Zhu, N. Samarth, and D. D. Awschalom, Phys. Rev. Lett. **97**, 126603 (2006).
[16] W. F. Koehl, M. H. Wong, C. Poblenz, B. Swenson, U. K. Mishra, J. S. Speck, and D. D. Awschalom, Appl. Phys. Lett. **95**, 072110 (2009).
[17] A. G. Aronov and Y. B. Lyanda-Geller, JETP Lett. **50**, 431 (1989).
[18] H.-A. Engel, E. I. Rashba, and B. I. Halperin, Phys. Rev. Lett. **98**, 036602 (2007).
[19] M.-H. Liu, S.-H. Chen, and C.-R. Chang, Phys. Rev. B **78**, 165316 (2008).
[20] B. Das, D. C. Miller, S. Datta, R. Reifenberger, W. P. Hong, P. K. Bhattacharya, J. Singh, and M. Jaffe, Phys. Rev. B **39**, 1411 (1989).
[21] G. Engels, J. Lange, Th. Schäpers, and H. Lüth, Phys. Rev. B **55**, R1958 (1997).
[22] T. Koga, J. Nitta, T. Akazaki, and H. Takayanagi, Phys. Rev. Lett. **89**, 046801 (2002).
[23] S. D. Ganichev, V. V. Belkov, L. E. Golub, E. L. Ivchenko, P. Schneider, S. Giglberger, J. Eroms, J. De Boeck, G. Borghs, W. Wegscheider, D. Weiss, and W. Prettl, Phys. Rev. Lett. **92**, 256601 (2004).
[24] V. K. Kalevich and V. L. Korenev, JETP Lett. **52**, 230 (1990).
[25] S. A. Crooker, M. Furis, X. Lou, P. A. Crowell, D. L. Smith, C. Adelmann, and C. J. Palmstrom, J. Appl. Phys. **101**, 081716 (2007).
[26] L. Meier, G. Salis, I. Shorubalko, E. Gini, S. Schön, and K. Ensslin, Nature Phys. **3**, 650 (2007).
[27] B. M. Norman, C. J. Trowbridge, J. Stephens, A. C. Gossard, D. D. Awschalom, and V. Sih, Phys. Rev. B **82**, 081304(R) (2010).
[28] J. Nitta, T. Akazaki, H. Takayanagi, and T. Enoki, Phys. Rev. Lett. **78**, 1335 (1997).
[29] S. Ghosh, D. W. Steuerman, B. Maertz, K. Ohtani, H. Xu, H. Ohno, and D. D. Awschalom, Appl. Phys. Lett. **92**, 162109 (2008).
[30] Y. Kato, R. C. Myers, A. C. Gossard, and D. D. Awschalom, Nature (London) **427**, 50 (2004).
[31] R. I. Dzhioev, K. V. Kavokin, V. L. Korenev, M. V. Lazarev, B. Ya. Meltser, M. N. Stepanova, B. P. Zakharchenya, D. Gammon, and D. S. Katzer, Phys. Rev. B **66**, 245204 (2002).
[32] J. M. Kikkawa and D. D. Awschalom, Phys. Rev. Lett. **80**, 4313 (1998).
[33] See Supplemental Material at http://link.aps.org/supplemental/10.1103/PhysRevLett.109.146603 for [brief description].
[34] K. Schmalbuch, S. Göbbels, Ph. Schäfers, Ch. Rodenbücher, P. Schlammes, Th. Schäpers, M. Lepsa, G. Güntherodt, and B. Beschoten, Phys. Rev. Lett. **105**, 246603 (2010).
[35] Although π rotation is completed at 4 ns, the minimum of Θ_F is seen at 3.7 ns. This shift results from a strong amplitude drop by the short T_2^*.
[36] R. J. Elliott, Phys. Rev. **96**, 266 (1954).
[37] M. I. D'yakonov and V. I. Perel, Sov. Phys. Solid State **13**, 3023 (1972).
[38] From the sample mobility of 5360 cm^2/Vs at $T = 30$ K we extract a momentum relaxation time less than 1 ps, which is significantly shorter than the ns time scale for spin manipulation.
[39] Among other things, 3D spin control requires quantitative analysis and mapping of strain anisotropy to CISP and 3D analysis of spin-orbit fields.